NUMERICAL MODELING OF A PARALLEL PLATE ELECTROWETTING-ON-DIELECTRIC (EWOD) DEVICE

by

KEVIN TULLY

Presented to the Faculty of the Graduate School of
The University of Texas at Arlington in Partial Fulfillment
of the Requirements
for the Degree of

MASTER OF SCIENCE IN MECHANICAL ENGINEERING

THE UNIVERSITY OF TEXAS AT ARLINGTON
MAY 2011

ACKNOWLEDGEMENTS

First I would like to thank my supervising professor Dr. Albert Y. Tong, for his advice and guidance. I appreciate the numerous hours he spent helping me, several meetings went longer than expected because it was important to him that I understand the concepts. Also I appreciate his flexibility and willingness to meet almost anytime if I needed help.

I would also like to thank my committee members, Dr. Hyejin Moon and Dr. Seiichi Nomura. I am extremely grateful for the teaching assistantship provided by the Mechanical and Aerospace Engineering Department at UTA. This assistantship made it possible to attend UTA and be able to focus on my research work.

Lastly, I would like to thank my family for their constant support. Especially my wife Nichole, for her consideration and cooperation during all of my research work.

April 15, 2011

ABSTRACT

NUMERICAL MODELING OF A PARALLEL PLATE
ELECTROWETTING-ON-DIELECTRIC
(EWOD) DEVICE

Kevin Tully, M.S.

The University of Texas at Arlington, 2011

Supervising Professor: Albert Y. Tong

Numerical modeling and simulations have been performed in this study that focuses on modeling the fluid dynamics of an Electrowetting-on-Dielectric (EWOD) device. The case to be modeled in the present study is a droplet cutting problem where a droplet is sandwiched between two plates of Teflon and an electrical actuation will cause the droplet to cut or split into two smaller droplets. A finite difference method has been used to solve the Navier-Stokes equations, along with the continuity equation. An algorithm used for tracking the free surface is the Volume of Fluid (VOF) method. Along with using the VOF method a Continuum Surface Force (CSF) model is implemented to accurately predict the physics of the surface tension on the free surface. The finalized algorithm used for solving the fluid flow is known as the Coupled Level Set – Volume of Fluid (CLSVOF) method. The physics of the fluid dynamics within a EWOD device have been investigated and adaptations have been made to the CLSVOF method to accurately predict the displacement and motion of the fluid. The accuracy of the numerical model has been validated using comparisons with published experimental data. A parametric study has been performed on the effects of various parameters.

TABLE OF CONTENTS

LIST OF ILLUSTRATIONS

Figure Page

LIST OF TABLES

CHAPTER 1

INTRODUCTION

1.1 Objective

Understanding the physics and problems related to Electrowetting-on-Dielectric (EWOD) devices has an enormous importance in current scientific research and future applications. The applications of this research are mostly biomedical as the use of Electro-wetting on dielectric devices have potential to be utilized in Lab-on-a-chip devices where precise controlling of a micro liquid's displacement is of great importance.

The main objective of this study is to provide a numerical method to accurately model the physics associated with a EWOD device while at the same time investigating the fluid dynamics. Even though there has been extensive hands-on research in a lab environment. There is a lack of research to predict the physics by numerical problem solving. Despite the fact that more is being learned and has to be learnt about EWOD devices the addition of a numerical model can act as a tool to help aid and accelerate the research that is currently going on across various university around the world, including the research here at University of Texas at Arlington being done by Dr. Hyejin Moon.

In the present study a 2-D free surface modeling code is being used that is written in FORTRAN. The choice to use a raw source code instead of a commercial CFD program was that it allowed full control over the physics of the problem and code modifications. For the present research an earlier code developed by Dr. Zhao Wang [1] while at University of Texas at Arlington under the supervision of Dr. Albert Tong was used. The code that Dr. Wang developed allows for three different free surface tracking methods; the Level Set (LS) method, the Volume of Fluid (VOF) method, and the Coupled Level Set – Volume of Fluid (CLSVOF) method. Of the three free surface tracking methods mentioned above, perusing use of the

CLSVOF method was the optimal choice for the current research. The code reconstructs the free surface using a Piecewise Linear Interface Construction (PLIC). The scheme used in this study to solve for surface pressure is the Continuum Surface Force (CSF) model. However Dr. Wang did develop a different scheme to solve for surface pressure known as the Pressure Boundary Method (PBM). But for the current research due to the physics of the EWOD device, the CSF model was the optimal choice.

Though there is a lack of numerical modeling of the fluid dynamics of EWOD devices, there has been a very extensive study done by Dr. Shawn Walker at University of Maryland, College Park [2] modeling the fluid dynamics of a EWOD using a Level Set method. The present numerical model focuses on the splitting of a droplet performed by a EWOD device. The study of EWOD splitting has been done numerically by Dr. Walker in [2] and experimentally by Dr. Moon in [3]. In this present study I am using the CLSVOF method to model the fluid dynamics of splitting droplet by a EWOD. The objective is to use an alternative method than done by Dr. Walker and hopes it shines new light and deepens the understanding of the physics related to a EWOD device.

1.2 Organization of Thesis

A review and explanation of the physics of a EWOD device and how it pertains to numerical modeling will be presented in Chapter 2. Chapter 3 will be a description of the numerical modeling approach used in the present study and the adaptations made to accommodate for modeling a EWOD device. The results and discussion will be reported in Chapter 4. Chapter 5 will contain the conclusions drawn from the results along with recommendations for future work.

CHAPTER 2

PHYSICS OF EWOD DEVICE

2.1 Introduction

An Electrowetting-on-Dielectric (EWOD) device is a device that uses electrical potential to displace a liquid. The device is very small and is on the micro scale (10^{-6} m). The dimensional specifics will be mentioned later in this study.

The device consists of two layers whose surfaces are parallel to each other. In the present study the device being modeled consists of a top layer of Teflon and a bottom layer of Teflon and dielectric silicon dioxide (SiO_2). The top layer acts as an electrical ground, while beneath the bottom layers are electrodes, which have the shape of squares and are 1.4 mm x 1.4mm. The electrodes are arranged in a grid pattern with very small spacing in between them. The voltage of each electrode can range from 0 to 25V. If the liquid being used contains an appreciable amount of ions, thus making the liquid electrically conductive, by applying voltage to an electrode, dielectric potential energy will be stored in the dielectric layer, which in our case is the bottom layer [4]. Figures 2.1 and 2.2 give a visual interpretation of the make-up of a EWOD device.

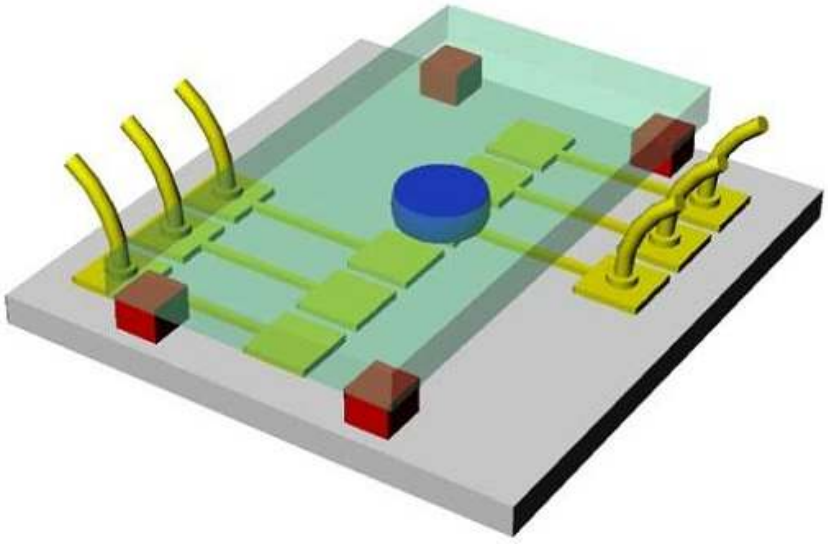

Figure 2.1. Schematic of sample EWOD device (source: [3]).

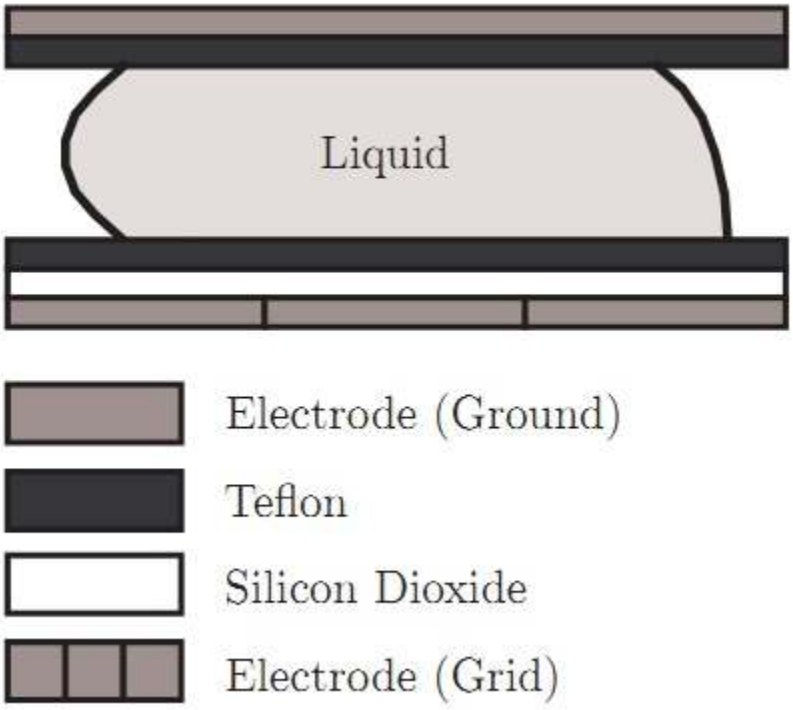

Figure 2.2 Cross-sectional view of the EWOD device (source: [2]).

2.2 Surface Tension and Curvature

To gain deeper knowledge of how a EWOD device displaces fluid it is imperative to know the relationship of surface tension and curvature. Surface tension, or surface force, is the driving force that causes the fluid to move within a EWOD device. The basic equation for surface force is given by:

$$p_s \equiv p - p_v = \sigma\kappa \tag{2.1}$$

where σ is the surface tension coefficient and κ is the curvature. The surface tension is a variable that is based upon the properties of the interface of the two fluids, while the curvature is based upon the geometry of the free surface of the liquid. Equation (2.1) shows that the surface tension is a function of the curvature of the free surface.

2.3 Contact Angle Actuation

As noted earlier the main objective of a EWOD device is to displace fluid on the micro scale using electrical actuation. To understand the physics of how this is done, understanding how the EWOD device can directly affect the contact angle that the fluid makes with its top and bottom plates is crucial. When an electrical potential is applied to an electrode, the contact angle between the liquid and the insulating dielectric layer changes due to the result of electrostatic forces [5]. The form of how the contact angle changes is directly a function of the magnitude of the applied voltage to the insulating dielectric layer, and is governed by the Young-Lippmann equation [6]:

$$\cos\theta_V = \cos\theta_o - \frac{\varepsilon_r \varepsilon_o V^2}{2\sigma h} \tag{2.2}$$

where θ_v is the contact angle under a given electric potential, θ_o is the contact angle under the absence of an electrical potential, ε_r is the relative permittivity of the dielectric layer, ε_o is the dielectric constant in a vacuum, and h is the thickness of the dielectric layer. In the present study the EWOD device in consideration for modeling only has a dielectric layer in the bottom

layer. Thus Equation (2.2) only applies to the bottom layer while the top layer remains at θ_o since there is no dielectric energy stored in the top layer. It must be noted that Equation (2.2) is based on the assumption that there is only a single plate in the EWOD device, unlike the experiment interested for the present study; where there is a top and bottom plate.

2.4 Contact Angle Saturation

The Young-Lippmann equation can be accurate in predicting contact angles. But once the voltage reaches a certain threshold the Young-Lippmann model does not match up with the experimental results [7]. This effect is known as contact angle saturation. Once the saturation limit is reached the contact angle will not vary even if the voltage is increased. To make sure the validity of the numerical scheme in the present study is still accurate, accounting for contact angle saturation is imperative. The proposed method is similar to the one used in [2]. There are two very important sets of data in [3]. These sets of data can be used to make an accurate model of how contact angle varies with voltage. The first set is data on how a water droplet on a single plate reacts to voltage actuation and the second set is data on how a droplet sandwiched between two plates reacts to voltage actuation. Figure 2.3 below shows the data along with the proposed model for determining contact angle.

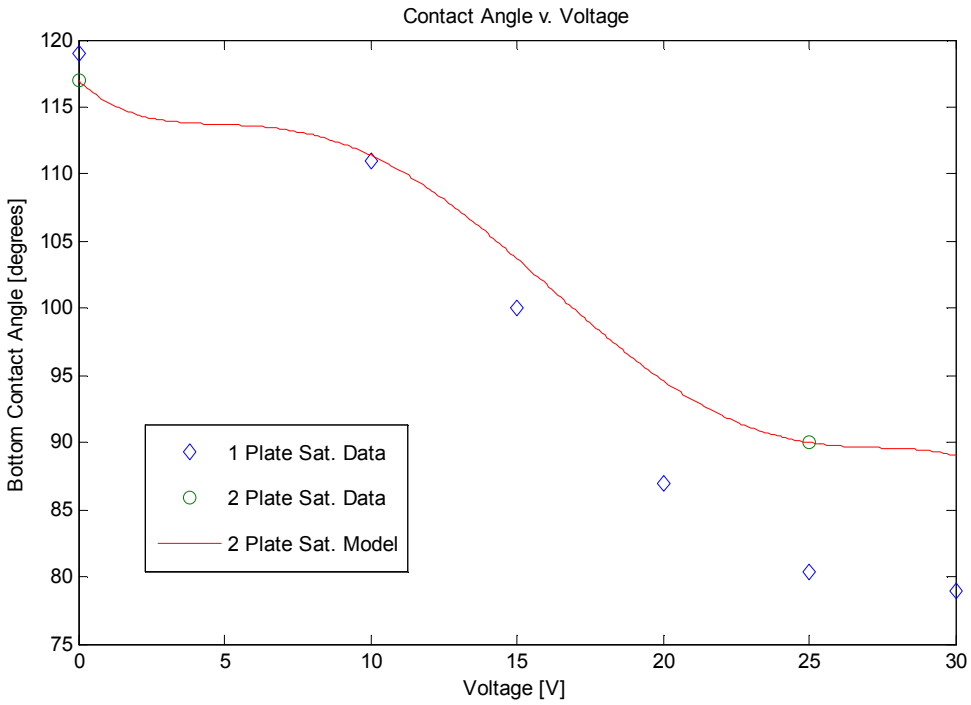

Figure 2.3. Contact angle versus voltage curve. The two sets of data represented by "o' and "◊" are experimental data from [3]. The 2 plate saturation model is derived using the data from [3].

The experimental data in [3] shows that the EWOD device where a droplet of water is sandwich in between two plates, that the bottom contact angle varies from 117° to 90° when the voltages changes from 0 to 25V. The one plate saturation curve in Figure 2.3 gives a good graphical understanding of contact angle saturation. From 25 V to 30 V the slope is very flat and the contact angle doesn't change much even if the voltage increases. The method to model contact angle saturation in the present study is to implement a method used in [2] where a linear mapping equation is used to map the 1 plate saturation data onto the 2 plate saturation data using the following equation:

$$\theta_{2p} = \frac{117° - 90°}{119° - 80.4°}\left(\theta_{1p} - 80.4°\right) + 90° \tag{2.3}$$

where θ_{2p} is the contact angle for 2 plate data and θ_{1p} is the contact angle for 1 plate data. Once the data is mapped using Equation (2.3) the 2 plate saturation model, as shown in Figure

2.3, is obtained by conducting a Vandermonde polynomial interpolation on the mapped data. The polynomial interpolation equation obtained is

$$\theta_b = -2.30\times10^{-5}V^5 + 1.84\times10^{-3}V^4 - 4.95\times10^{-2}V^3 + 4.84\times10^{-1}V^2 - 2.06V + 117 \quad (2.4)$$

where θ_b is the bottom contact angle, which is in contact with the dielectric bottom layer, and V is the applied voltage.

2.5 Contact Angle Hysteresis

A droplet of water on an ideal smooth surface should have a unique contact angle regardless of the direction of the fluid. But the surfaces on a EWOD device are not perfectly smooth. These surfaces are heterogeneous and contain roughness. The values of the measured contact angles will vary due to the roughness of the surface [8]. Figure 2.4 is the best way to visualize and understand contact angle hysteresis. If a droplet of water is placed on a plane surface that is tilted, the droplet will move. When the droplet moves due to gravity the contact angle on the advancing edge will always be greater than the contact angle on the receding edge [9]. However once a droplet is at rest and is not moving the droplet will have the same contact angle on both sides, since friction in a fluid cannot supply a static force [10].

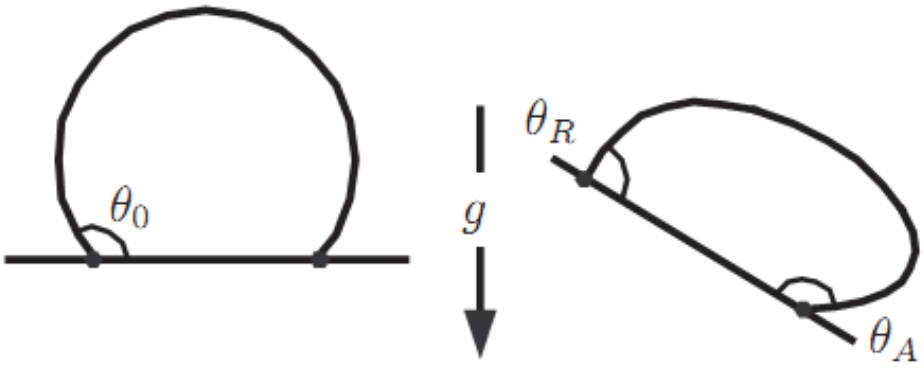

Figure 2.4. Illustration of contact angle hysteresis. θ_o is the nominal (equilibrium) contact angle when the surface is level. When the surface is tilted, θ_R is the receding contact angle that will be less than θ_o, and θ_A is the advancing contact angle than will be greater than θ_o. (source: [2]).

The difference between the receding and advancing contact angle is the value of hysteresis. For the present study a new variable, Δ_{hys}, will be defined to represent how the effect of hysteresis is quantified.

$$\Delta_{hys} \equiv \theta_o - \theta_R = \theta_A - \theta_o \tag{2.5}$$

By observing Equation (2.5) the assumption is made that when the affect of hysteresis is present that the value of the receding and advancing contact angles deflect from θ_o by the same amount. The physics of contact angle hysteresis have to be included in the present numerical model to provide accurate results. Details of how contact angle hysteresis is incorporated numerically will be discussed in chapter 3.

2.6 Summary

As mentioned in Section 2.2, surface tension is the driving force. Also it should be known that surface tension and curvature have a linear relationship given by Equation (2.1). When a change is made to the contact angle of the fluid on the bottom dielectric layer, by result

of the geometry of the free surface, the curvature must change. In can be shown by using basic geometry that the non-dimensional curvature can be described by

$$\kappa_z = -\left(\cos\theta_t + \cos\theta_b\right) \tag{2.6}$$

where κ_z is the curvature about the z-axis, and θ_t and θ_b are the top and bottom contact angles respectively. It must be noted that equation (2.6) is based on the assumption that liquid-gas interface has a circular cross section [2]. Figure 2.5 shows graphically how contact angles and curvature are related.

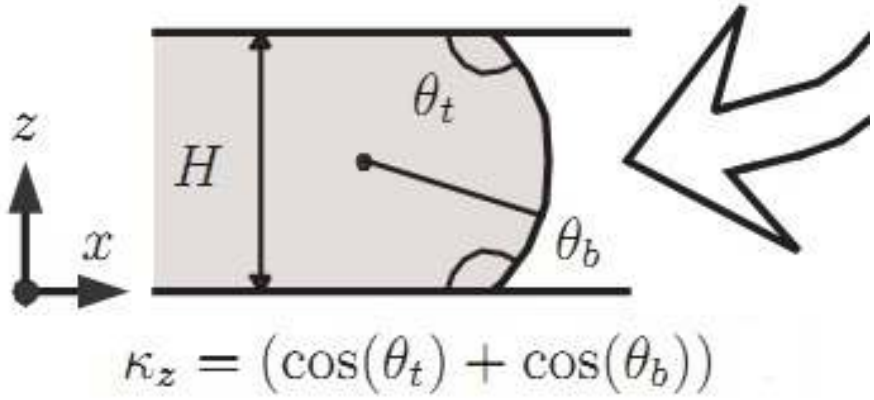

Figure 2.5. A view of the liquid-gas interface on the z-x plane. (source: [2]).

In the present numerical model proposed, Equations (2.1), (2.4), and (2.6) are used to predict the surface tension as a function of the applied voltage. This is the key to understanding the physics of a EWOD device.

Figure 2.6 shows a droplet where approximately half of its volume is located on an electrode that is OFF (0 V) and the other half is located on an electrode that is ON (25 V). Since the bottom contact angle in the ON region is less than the bottom contact angle in the OFF region (as predicted by Figure 2.3 and Equation (2.4)) the surface tension in the OFF region will be greater than the surface tension in the ON region. This difference in surface tension will inherently cause the droplet to move from the OFF region to the ON region.

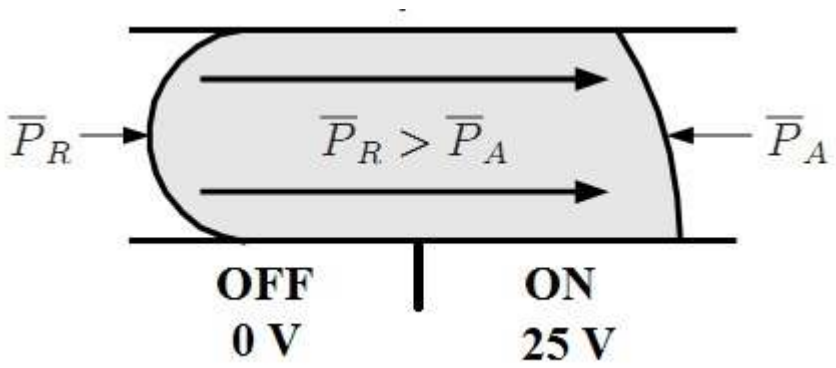

Figure 2.6. A visual demonstration of motion of a droplet in a EWOD device. $\overline{P}_R$ represents the pressure on the receding end, and $\overline{P}_A$ represents the pressure on the advancing end. Note how $\overline{P}_R > \overline{P}_A$ and thus the droplet will move from the left to right.

Now a basic understanding of the physics of a EWOD device has been described along with how these physics pertain to numerical modeling and predicting its motion. In next chapter a discussion of the details of the numerical scheme in the present study and its execution related to the EWOD device will be given.

CHAPTER 3

NUMERICAL MODELING

3.1 Governing Equations

The basis for the numerical modeling in the present study is solved using 2D fluid flow in an Eulerian frame. The governing equations used are the continuity equation for incompressible flow,

$$\nabla \bullet \vec{V} = 0 \tag{3.1}$$

and the transport of fluid momentum,

$$\frac{\partial \vec{V}}{\partial t} + \nabla \bullet \left(\vec{V}\vec{V} \right) = -\frac{1}{\rho}\nabla p + \frac{1}{\rho}\nabla \bullet \tau + \vec{g} + \frac{1}{\rho}\vec{F}_b \tag{3.2}$$

where ρ is the fluid density, p is the scalar pressure, τ is the viscous stress tensor, $\vec{F}_b$ is a body force, and $\vec{g}$ is the gravitational acceleration. For Newtonian fluid, the viscous stress tensor τ is

$$\tau = 2\mu S \tag{3.3}$$

$$S = \frac{1}{2}\left[\left(\nabla \vec{V} \right) + \left(\nabla \vec{V} \right)^T \right] \tag{3.4}$$

where S is the rate-of-strain tensor and μ is the coefficient of dynamic viscosity. The first step needed to solve the algorithm for fluid flow is to discretize the momentum Equation (3.2), which yields:

$$\frac{\vec{V}^{n+1}-\vec{V}^{n}}{\delta t}=-\nabla\bullet\left(\vec{V}\vec{V}\right)^{n}-\frac{1}{\rho^{n}}\nabla p^{n+1}+\frac{1}{\rho^{n}}\nabla\bullet\tau^{n}+\vec{g}^{n}+\frac{1}{\rho^{n}}\vec{F}_{b}{}^{n} \tag{3.5}$$

where the superscripts n and n+1 represent time step of n and n+1 , respectively. Equation (3.5) is broken up into two steps. This is known as the two-step projection method [11]; which is given by:

$$\frac{\vec{\tilde{V}}-\vec{V}^{n}}{\delta t}=-\nabla\bullet\left(\vec{V}\vec{V}\right)^{n}+\frac{1}{\rho^{n}}\nabla\bullet\tau^{n}+\vec{g}^{n}+\frac{1}{\rho^{n}}\vec{F}_{b}{}^{n} \tag{3.6}$$

and

$$\frac{\vec{V}^{n+1}-\vec{\tilde{V}}}{\delta t}=-\frac{1}{\rho^{n}}\nabla p^{n+1} \tag{3.7}$$

where $\vec{\tilde{V}}$ is the intermediate value of velocity, between the time at n and the time at n+1. In the first step, $\vec{\tilde{V}}$ is computed from the values of the previous time step: advection, viscosity, gravity, and body forces are approximated at t = n. The second step of the two step projection method requires taking the divergence of Equation (3.7) and imposing the zero-divergence of $\vec{V}^{n+1}$ because of the discretized continuity equation, which is:

$$\nabla\bullet\vec{V}^{n+1}=0 \tag{3.8}$$

Then velocity field $\vec{V}^{n+1}$ is projected onto a zero-divergence vector field resulting in a pressure Poisson equation (PPE),

$$\nabla \bullet \left[\frac{1}{\rho^n} \nabla p^{n+1} \right] = \frac{\nabla \bullet \vec{\vec{V}}}{\delta t} \tag{3.9}$$

The Incomplete Cholesky Conjugate Gradient (ICCG) solution technique is used to solve Equation (3.9). This solution results in acquiring the vector field of the next time step, t = n + 1, which completes the two step projection method.

3.2 Free Surface Tracking

In the computer code of the present study, the free surface is tracked by two methods called Volume of Fluid (VOF) and Level Set (LS). Both of the methods mentioned can handle 2-D fluid flow problems that require fluid deformations that have large topological changes.

The free surfaces in the VOF method are reconstructed by using a scalar field $F\left(\vec{x},t\right)$, which is defined as follows:

$$F\left(\vec{x},t\right) = \begin{cases} 1, & \text{in the fluid;} \\ 0 < F < 1, & \text{at the interface;} \\ 0, & \text{outside the fluid;} \end{cases} \tag{3.10}$$

From this definition, the VOF function can be interpreted that it represents non-dimensional density of the fluid in a cell. To understand Equation (3.10) better and how the VOF method quantifies the free surface refer to Figure 3.1 below.

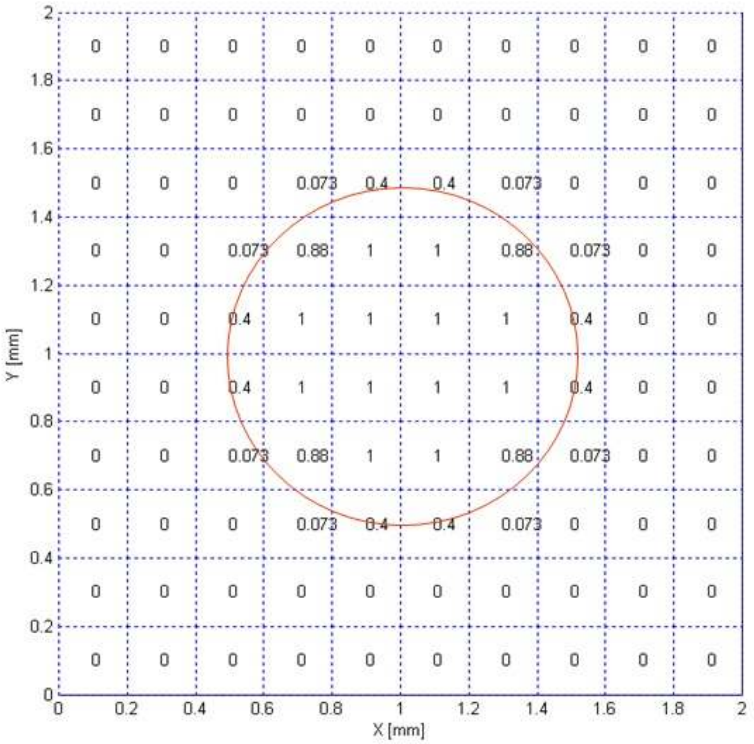

Figure 3.1. Plot of VOF method. In this figure the red line represents the free surface of a circle, while the values in each individual cell come from Equation (3.10).

In the VOF method, the governing equation is given below in which F is treated as a Lagrangian invariant:

$$\frac{DF}{Dt} = \frac{\partial F}{\partial t} + \left(\vec{V} \bullet \nabla\right) F = 0 \tag{3.11}$$

Free surfaces in the VOF method are tracked by using a scheme that was developed by Hirt and Nichols [12]. This method uses the donor-accepter differencing to track the movement of the free surfaces. The exact solution to Equation (3.11) would yield

$$\left(\frac{\partial F}{\partial t}\right)_{exact} = -\left(\vec{V} \bullet \nabla\right) F \tag{3.12}$$

this refers to the exact analytical solution of the partial differential equation. A better approach would be to use a conservative form of Equation (3.12) , which is as follows:

$$\left(\frac{\partial F}{\partial t}\right)_{calc} = -\left(\nabla \bullet \vec{V}\right) F - \left(\vec{V} \bullet \nabla\right) F \tag{3.13}$$

where $\left(\frac{\partial F}{\partial t}\right)_{calc}$ refers to the numerical solution of the partial differential equation (3.11). Note how the velocity divergence is not zero, because $\nabla \bullet \vec{V}$ is a small value due to the machine epsilon [11]. The combination of Equations (3.12) and (3.13), gives the following result:

$$\left(\frac{\partial F}{\partial t}\right)_{exact} = \left(\frac{\partial F}{\partial t}\right)_{calc} + \left(\nabla \bullet \vec{V}\right) F \tag{3.14}$$

Equation (3.14) can reduce the numerical error in the VOF advection calculations.

To begin the advection process the intermediate value $\widetilde{F}$ must be defined as:

$$\widetilde{F} = F^n - \delta t \nabla \bullet \left(\vec{V} F^n\right) \tag{3.15}$$

The advection process can be completed using a divergence correction which results in:

$$F^{n+1} = \widetilde{F} + \left(\nabla \bullet \vec{V}\right) F^n \tag{3.16}$$

At the beginning of the each computational cycle, fluid volumes are initialized in each cell according to the free surface geometry specified in the *input* file. The interface is then discretized to continue the calculations and the discrete fluid volume data is used by future computations. A reconstruction algorithm know as Piecewise Linear Interface Calculation (PLIC) , which was developed by Lu [13] at University of Texas at Arlington, is used to reconstruct the free surface. The PLIC algorithm reconstructs the free surface interface as a linear line segment

in each individual cell. The angular orientation of the line segment is in such a way that the fraction of the fluid volume in each cell is equal to, $F\left(\vec{x},t\right)$, thus still preserving the mass. There is however another algorithm called the Nichol-Hirt (NH) algorithm, which reconstructs the interface using vertical and horizontal line segments in each individual cell. The NH algorithm creates a very unsmooth surface. The PLIC algorithm has been validated that it shows less distortion than the NH algorithm.

The free surfaces in the LS method are reconstructed using a distance function, $\phi\left(\vec{x},t\right)$, which represents the distance magnitude from the cell's center to the nearest free surface [14]. The sign of the LS function is defined as follows:

$$\phi\left(\vec{x},t\right)=\begin{cases}>0, & \text{outside the fluid;}\\ =0, & \text{at the interface;}\\ <0, & \text{in the fluid;}\end{cases} \tag{3.17}$$

To understand Equation (3.17) better and how the LS method quantifies the free surface refer to Figure 3.2 below.

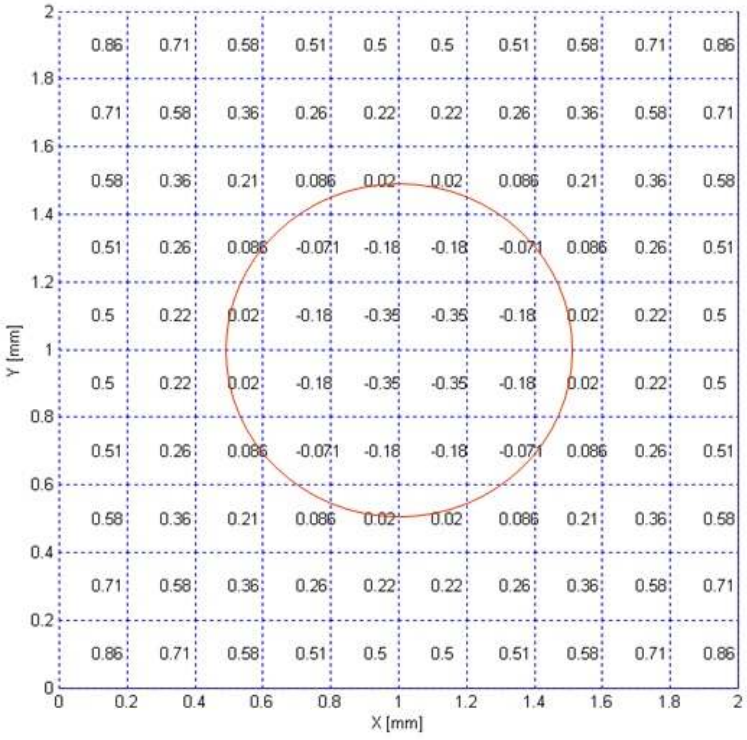

Figure 3.2. Plot of LS method. In this figure the red line represents the free surface of a circle, while the values in each individual cell come from Equation (3.17).

The next step is to advance the LS function using the following equation:

$$\frac{D\phi}{Dt} = \frac{\partial \phi}{\partial t} + \left(\vec{V} \bullet \nabla\right)\phi = 0 \tag{3.18}$$

Due to its advantages in computing curvature the LS function is used to calculate the normal of interface surface using the following formula:

$$\hat{n} = \frac{\nabla \phi}{\left|\nabla \phi\right|} = \nabla \phi \tag{3.19}$$

It is possible however that the LS function may become irregular and increasing its gradient will result in numerical errors. To combat these possible numerical errors and minimize their effect, the LS function can be reinitialized [15] using the following equation:

$$\frac{\partial \phi}{\partial t} = \frac{\phi_0}{\sqrt{\phi_0{}^2 + h^2}} \left(1 - |\nabla \phi|\right) \tag{3.20}$$

where ϕ_0 is the LS function of the previous time step, t is the artificial time, and h is the grid spacing.

The LS function can be implemented to directly compute the local curvature using:

$$\kappa = \nabla \bullet \nabla \phi \tag{3.21}$$

One of the main, advantageous differences of the LS function compared to the VOF function is that it is a smooth function, whereas the VOF function value jumps from cell to cell without any continuity. Knowing this it is expected that the LS function will show better results calculating the local curvature or gradient of the free surface.

As mentioned in Chapter 1 the proposed method for tracking the free surface is the Coupled Level Set Volume of Fluid (CLSVOF) method as developed by Wang [1] at the University of Texas at Arlington. The CLSVOF method is a hybrid scheme that uses the advantages of the VOF and LS free surfaces tracking methods, while minimizing their weaknesses.

The CLSVOF method adopts the VOF method for tracking the free surface using Equation (3.11). While the Level Set (LS) method is used for computation of the normal vector to the free surface and the local curvature using Equations (3.19) and (3.21). Although the VOF method preserves mass at nearly 100%, it does however lack the accuracy in computing the normal vector and local curvature. This lack of accuracy is from the mathematics of the VOF function, which is a jump function compared to the LS function, which is a smooth function [16]. This is reasoning behind using the LS method.

Figure 3.3 below shows a flow chart with the basic steps taken to solve the fluid flow using the CLSVOF method. One of the main disadvantages of this scheme is that it employs more computational load on the computer since the scheme calculates both the VOF and LS function [17].

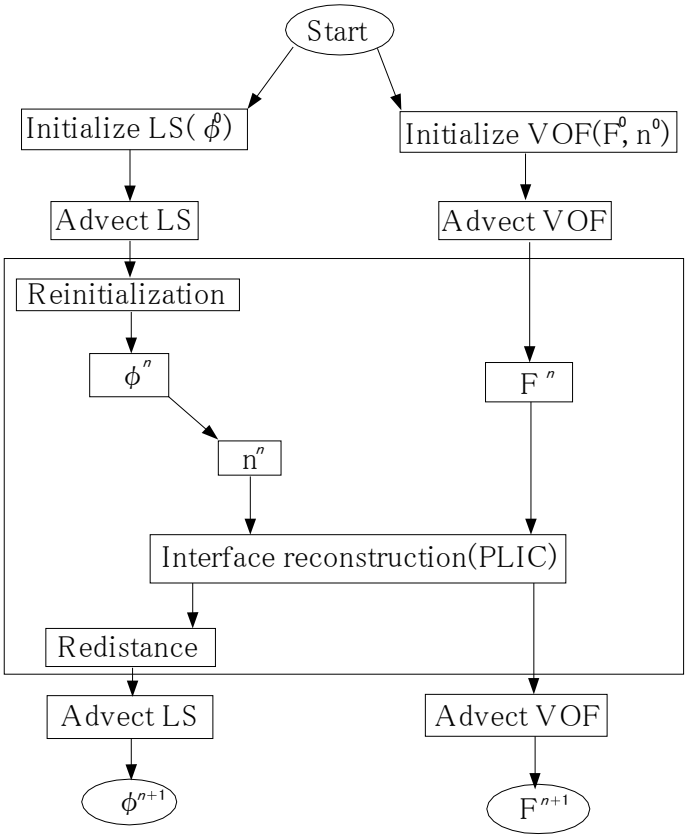

Figure 3.3. A flow chart and overview of the CLSVOF method.

3.3 Surface Tension Modeling

The Continuum Surface Force (CSF) method is implemented in the current study to model the surface tension at the free surface. The CSF method is a unique approach which was proposed by Brackbill, Kothe and Zemach [18]. In the present numerical model the viscous effects are neglected at the free surface and the surface tension coefficient, σ, is assumed to be constant. The stress boundary condition can be described by Equation (2.1), which is also known as Laplace's formula. Other methods, such as used in NASA-VOF2D [19], have used Equation (2.1) directly to solve for the surface pressure, but the CSF method uses instead a volume surface force, $\vec{F}_{sv}\left(\vec{x}\right)$, that is given by

$$\vec{F}_{sv}\left(\vec{x}\right) = \sigma\kappa\left(\vec{x}\right)\frac{\nabla\tilde{c}\left(\vec{x}\right)}{\left[c\right]} \tag{3.22}$$

where $\tilde{c}\left(\vec{x}\right)$ is the color function, which represents the fluid-gas interface, and $\left[c\right]$ is a normalizing factor, which biases the surface force toward the fluid side of the transition region. For the present numerical study the LS function, $\phi\left(\vec{x},t\right)$, will be used to represent the fluid-gas interface.

$$\tilde{c}\left(\vec{x}\right) = \phi\left(\vec{x},t\right) \tag{3.23}$$

By combining Equations (3.19), (3.22), and (3.23) an updated form for the volume surface force is acquired:

$$\vec{F}_{sv} = \sigma\kappa\left(\vec{x}\right)\delta\left(\vec{x}\right)\hat{n} \tag{3.24}$$

where $\delta\left(\vec{x}\right)$ is a delta function that is concentrated at the interface. The volume force, $\vec{F}_{sv}$, is a body force and can be replaced by $\vec{F}_b$ in Equation (3.2).

The term, $\kappa\left(\vec{x}\right)$, in Equation (3.24) represents the mean curvature of the droplet at location $\vec{x}$. The computation of the mean curvature requires use of the curvature about the x-y plane, κ_{xy}, and the curvature about the z-axis, κ_z. Figure 3.4 shows a graphical understanding of the how these two curvatures are implemented.

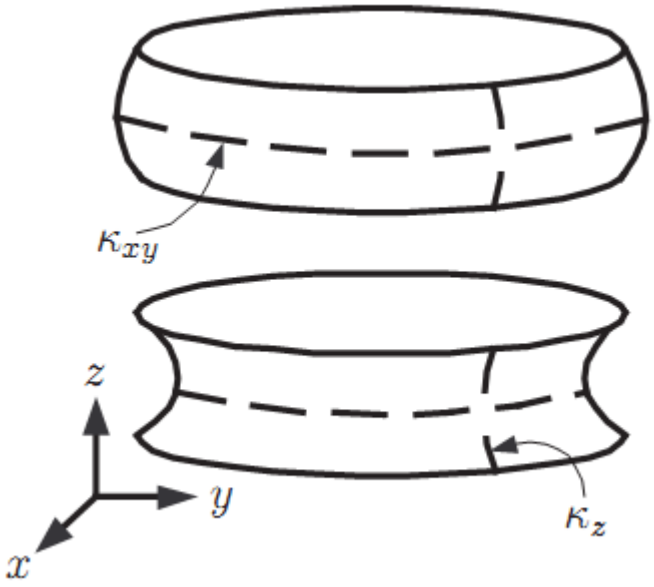

Figure 3.4. 3-D view of κ_{xy} and κ_z. (source: [2]).

In the present study Equation (3.21) is used to estimate the curvature about the x-y plane, κ_{xy}, and Equation (2.6) is used to estimate the curvature about the z-axis, κ_z. Computation of the mean curvature is given by,

$$\kappa\left(\vec{x}\right) = \kappa_{xy} + \frac{L}{H}\kappa_z \tag{3.25}$$

where L is a specified length scale. Since the channel spacing is so small, the $\frac{L}{H}$ term is needed to accurately approximate the surface tension [2]. By combining Equations (3.24) and (3.25), the finalized surface volume force equation is acquired.

$$\vec{F}_{sv} = \sigma\left(\kappa_{xy} + \frac{L}{H}\kappa_z\right)\delta\left(\vec{x}\right)\hat{n} \tag{3.26}$$

The CSF method makes use of the fact that the surface tension varies continuously across the fluid-gas interface, as opposed to using Equation (2.1) directly which involves a discontinuity at the free surface. It is not suitable to use in a finite-difference scheme where the surface tension could "jump" at the free surface. It is more reasonable to use a method where the surface tension act everywhere throughout the transition region using the volume force, $\vec{F}_{sv}$, in the CSF method.

3.4 Electrical Actuation Modeling

The original computer code being applied for the current study has no option of including an electrode and applying voltage to the fluid flow field. It is necessary to manually alter the code to account for an electrode's location and its applied voltage. The proposed method to remedy this problem is for each electrode to set up 4 virtual walls, since an electrode is a square, one for each side as shown in Figure 3.5.

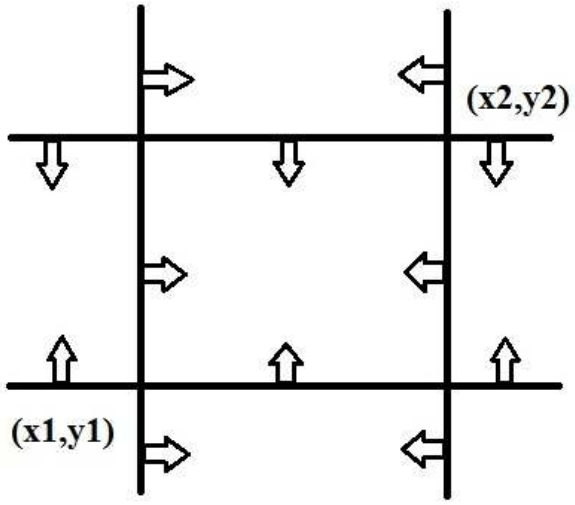

Figure 3.5. Visual implementation of defining electrode location.

The coordinates (x1,y1) and (x2,y2) are the bottom left and top right locations of the electrode respectively. By knowing these two locations, the dimensions of the electrode and where it is located in mesh can be acquired. The way to numerically implement this idea is to scan across the x-axis followed by scanning across the y-axis. When scanning, the computer program checks to see if a node is on the actuated electrode side (in Figure 3.5 the side where the arrows are pointing) of each virtual wall. If any node during this scan is located within the correct side of all four virtual walls, that node for the duration of the simulation will be referred to as in an ON location. For the current model only the electrodes that are actuated during the experiment need to me accounted for. If an electrode is not defined, that area is assumed to have 0V applied, or in an OFF region. This is achieved by using multiple *for* loops and nested *if* statements in FORTRAN.

3.5 Hysteresis Modeling

For many 2-D fluid flow problems the effects of hysteresis are negligible and thus there is no need to accurately model them in a computer code. However due to the physics and

geometry of a EWOD device accounting for hysteresis is imperative. It has been shown in [2] that including the physics of hysteresis has a profound effect on the accuracy of the numerical model .

The first step to modeling the hysteresis is to determine whether the fluid is advancing or receding. This can be established by the following equation:

$$\hat{n} \bullet \vec{V} = \begin{cases} < 0, & \text{Receding} \\ > 0, & \text{Advancing} \end{cases} \tag{3.27}$$

Equation (3.27) is applied to the fluid on the free surface. Once the direction of the fluid is determined the next step is to manually alter the contact angles with the top and bottom layers on the x-z plane. If fluid on the free surface has been determined to be receding then the following equation is used,

$$\begin{aligned} \widetilde{\theta}_{b,R} &= \theta_t - \Delta_{hys}, \\ \widetilde{\theta}_{t,R} &= \theta_b - \Delta_{hys} \end{aligned} \tag{3.28}$$

where θ_t is the top contact angle, remains at 117°, and θ_b is the bottom contact angle which follows Equation (2.4). If the fluid on the free surface has been determined to be advancing then the following equation is used,

$$\begin{aligned} \widetilde{\theta}_{b,A} &= \theta_t + \Delta_{hys}, \\ \widetilde{\theta}_{t,A} &= \theta_b + \Delta_{hys} \end{aligned} \tag{3.29}$$

After the contact angles have been adjusted by Equations (3.28) and (3.29), $\widetilde{\theta}_{b,R}$, $\widetilde{\theta}_{t,R}$, $\widetilde{\theta}_{b,A}$, and $\widetilde{\theta}_{t,A}$ are then incorporated into equation (2.6) to compute the curvature about the z-axis. Figure 3.6 is a cross-sectional view of a EWOD device when hysteresis is present.

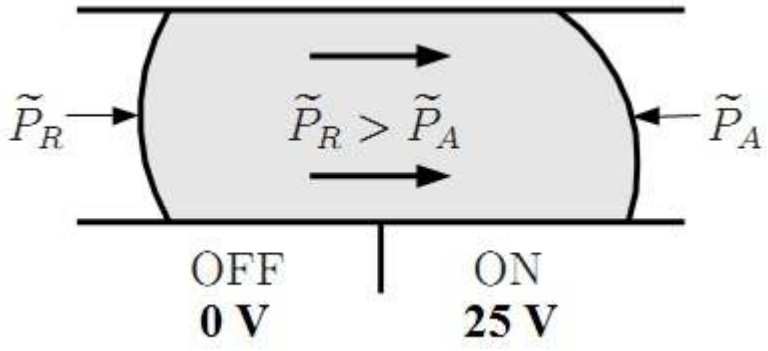

Figure 3.6. Cross sectional view of EWOD including hysteresis.

In Figure 3.6, $\widetilde{P}_R$ and $\widetilde{P}_A$ represent the receding and advancing surface pressure when hysteresis is included in the numerical model. By observation of Figure 3.6 and Equations (3.28) and (3.29), the pressure difference between the left and right sides is reduced when hysteresis is incorporated. This reduced pressure difference retards the motion of the fluid and thus the fluid does not accelerate as fast as if the hysteresis effect was ignored.

From own numerical experiments applying Equations (3.28) and (3.29) does not fully model the effect of hysteresis. The fluid accelerated faster than observed in [3]. To achieve the full effect of hysteresis in the present study, an additional method was included that is similar to that devised in [2]. The proposed method is to manually alter the fluid acceleration terms. In the original CLSVOF method developed by Wang [1] fluid acceleration was computed by,

$$\rho \frac{\partial \vec{V}}{\partial t} = \vec{F}_{sv} \tag{3.30}$$

The fluid acceleration terms can be altered by scaling Equation (3.30) by a constant,

$$\rho \frac{\partial \vec{V}}{\partial t} = K_{hys} \vec{F}_{sv} \tag{3.31}$$

where K_{hys} is a constant smaller than one. The best attempt at estimating the effect of slowing down the fluid acceleration is to use the volume force. K_{hys} can be defined by the ratio of the volume force when hysteresis is included to the volume force ignoring hysteresis. Also since the relationship between the volume force and curvature is linear by Equation (3.24), curvature can be used to define the constant K_{hys},

$$K_{hys} = \frac{\left(\Delta\vec{F}_{sv}\right)_{hys}}{\left(\Delta\vec{F}_{sv}\right)} = \frac{\widetilde{\kappa_R} - \widetilde{\kappa_A}}{\kappa_R - \kappa_A} \tag{3.32}$$

where $\widetilde{\kappa_R}$ and $\widetilde{\kappa_A}$ are the curvatures on the receding and advancing sides of the fluid respectively when the effect of hysteresis is included. By combining equations (2.6), (3.28), (3.29) and (3.32) the estimate for K_{hys} is given by,

$$\begin{aligned}
\left[num\right] &= \left[\cos\left(\widetilde{\theta}_{t,R}\right) + \cos\left(\widetilde{\theta}_{b,R,0V}\right) - \cos\left(\widetilde{\theta}_{t,A}\right) - \cos\left(\widetilde{\theta}_{b,R,25V}\right)\right] \\
\left[den\right] &= \left[\cos\left(\theta_t\right) + \cos\left(\theta_{b,0V}\right) - \cos\left(\theta_t\right) - \cos\left(\theta_{b,25V}\right)\right] \\
K_{hys} &= \frac{\left[num\right]}{\left[den\right]}
\end{aligned} \tag{3.33}$$

where the voltage subscripts for the bottom contact angles represent the amount of applied voltage. In Chapter 4, a study has been performed to estimate the appropriate Δ_{hys}, and resulting K_{hys}, to ensure an accurate model.

CHAPTER 4

RESULTS AND DISCUSSION

4.1 Introduction

As mentioned in previous chapters, the present study uses a CLSVOF scheme to track free surfaces. Also incorporated into the code are the physics of hysteresis and its effect on the fluid flow within a EWOD device. To demonstrate the superiority and effectiveness of the CLSVOF scheme it will be compared to results from using the LS method only. Furthermore, simulations will be run without the included the effect of hysteresis and comparisons will be made to validate its inclusion in the code and whether or not it affects the results. Once the final numerical method has been established the results will be compared with previous experimental results obtained by Dr. C.J. Kim and Dr. Hyejin Moon [3] at UCLA.

A grid refinement study has been performed whose goal is to optimize the mesh used. The size of the mesh, the pinch-off time, mass conservation, fluid displacement and the overall curvature and shape of the simulated drop within the EWOD will be used to determine the optimal grid size.

A parametric study has been done which examines the effects of the hysteresis angle deflection, and other fluid properties such as density, viscosity, and surface tension coefficient. The computations carried out in this numerical study solve the full transient Navier-Stokes equation in a 2D Cartesian coordinate system adequate for simulating the flow of a droplet in a EWOD device.

4.2 Problem Set-Up

The exact physical EWOD problem being solved is known as a droplet cutting problem. The same problem has been numerically solved in [2] and experimentally studied in [3]. The results from those studies will be used for comparison with the numerical results obtained in the present study. Figure 4.1 shows the initial free surface and electrode locations and prescribed voltage for the droplet cutting problem.

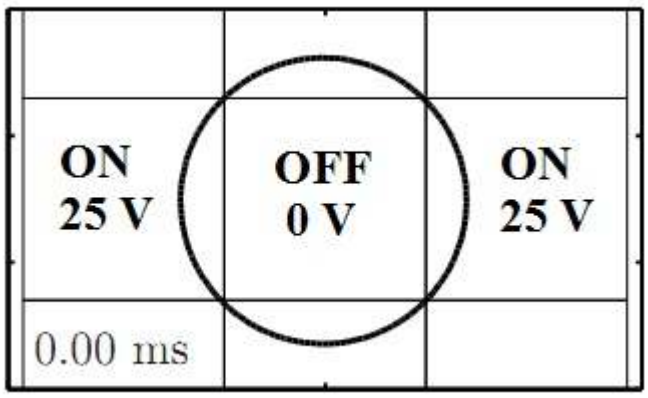

Figure 4.1. The initial set-up for the droplet cutting problem.

As shown in Figure 4.1, the initial free surface is a circle whose location is centered in the middle electrode, and its diameter is approximately the length of the diagonal of the electrode. Each electrode is a 1.4 mm x 1.4 mm square. Only the two electrodes to the left and right of the initial drop are actuated by a voltage of 25 V, while the middle electrode is not actuated and remains at 0 V for the remainder of the experiment. Theoretically the droplet should move from the OFF region to the ON regions due to the induced pressure difference. For the current simulations the fluid modeled is distilled water. Though the properties of water are dependent upon various physical effects such as temperature and pressure, the exact values reported in [2] are used in the present numerical study in order to give the most optimal comparisons. These values are given in Table 4.1.

Table 4.1. Physical parameters of EWOD experiment.

Parameter	Symbol	Value
Density	ρ	996.93 kg/m^3
Dynamic Viscosity	μ	0.89 g/m*s
Surface Tension Coeff.	σ	0.07199 J/m^2
Channel Height	H	70 μm
Electrode Length	L_{elec}	1.4 mm
Length Scale	L	4.2 mm

4.3 LS Method

As mentioned in previous chapters the CLSVOF method is used to track the free surface of the liquid. It is also known that the LS method does not efficiently preserve mass well. To prove that the LS method is not the optimal choice for the present research, modeling the EWOD using only the LS free surface tracking method needed to be investigated. Figure 4.3 shows the results of the simulation. As expected, in Figure 4.3(a) the droplet starts to initially spread and enter into the electrodes actuated by 25 V. Figure 4.3(b) shows that while the droplet is being elongated, a neck starts to form. The neck becomes so thin that it snaps due to capillary instability. After the neck snaps two droplets are formed and they eventually rest upon both of the 25 V electrodes. At first glance it appears that the LS method accurately predicted the physics associated with the droplet cutting problem. However while the simulation is run, the droplet of water starts to lose mass. When the simulation reaches 85 ms, as in Figure 4.3(b), 45% of the droplets initial mass is lost. Also when the simulation is finalized at 116 ms, as in Figure 4.3(c), 76% of the droplets initial mass is lost. This severe amount of loss of mass is due to inherent nature of the LS method and its lack of mass conservation. It must also be noted

that the LS method is still a viable and reputable free surface tracking method. The current problem and numerical alterations mentioned in Chapter 3, exacerbated the LS method's lack of mass conservation. These current findings steered the current research to search more a more effective free surface tracking method. Ultimately the CLSVOF method was chosen to be used for free surface tracking.

4.4 No Hysteresis

Through researching the literature, the effect of hysteresis can have a profound impact on the results of a fluid flow problem. Most notably in [2], a comparison with modeling done using hysteresis and ignoring hysteresis was conducted. The hysteresis had a drastic effect and was imperative to an accurate model. However the present study is incorporating a CLSVOF free surface tracking method with the CSF method to model surface tension. To gain a deeper understanding of the physics, a study has been preformed that ignores contact angle hysteresis. This current study ignoring hysteresis was conducted using the CSLVOF method.

Figure 4.4 shows the simulation conducted where the effect of hysteresis was not included in the model. Chapter 3 mentions that hysteresis retards the motion of the fluid. For this simulation the pressure difference caused by the EWOD is actually much larger than actual reality. After only 7 ms, Figure 4.4(a), a neck is starting to form. Because the fluid is moving fast the neck hasn't had a chance to become thin and a bulge has formed in the middle of the 0 V electrode. By 25 ms, Figure 4.4(b), the neck is now thinning and fluid is about to pinch off. When pinch-off occurs it doesn't happen in the middle of the 0 V electrode as expected. The pinch-off occurs closer towards the end of each bulge on both of the 25 V electrodes. The result is three satellite droplets resting one each on top of the electrodes as shown in Figure 4.4(c). The pinch-off time, t^*, for this simulation is 27 ms, which is approximately 4.8 times faster than the experiment from [3]. In the current simulations it was noticed that the force due to the electrical actuation caused the curvature about the z-axis, κ_z, to dominate the curvature on the

x-y plane. The current simulations ignoring the contact angle hysteresis have validated the need to include hysteresis in the present numerical model.

4.5 Grid Refinement Study

The simulations ran in Sections 4.3 and 4.4 have validated the current numerical model. Using a CLSVOF method for surface tracking, and also incorporating the physics of contact angle hysteresis has been proven to be the optimal model. The next step is to optimize the computational mesh. Since the current problem does not require using 3-D axi-symetrical mesh, a Cartesian coordinate, rectangular mesh with even spacing has been chosen. To save the computational workload a symmetric boundary condition about the x-axis has been formed. Essentially only half of the domain shown in Figure 4.1 will actually be computed. Through numerous simulations, it has been determined that buffer regions need to be established to achieve accurate and physically reasonable results. The choice was to use a buffer half the length of an electrode, 0.7 mm. Table 4.2 shows various mesh sizes and the resulting pinch off time, t^*.

Table 4.2. Grid refinement study.

Grid Resolution	t^* **[ms]**
80 x 30	116.4
96 x 36	127.4
112 x 42	136.5
128 x 48	139.9
144 x 54	141.1

The result from Table 4.2 shows that finer the mesh the greater the pinch off time. While a coarser mesh such as 80 x 30 results in inaccurate results, surprisingly a finer mesh wasn't the most optimal choice. The pinch-off time of the finer mesh did not correlate well with the experimental results. The choice for the current model was to pursue using a 112 x 42 mesh. Although the 96 x 36 mesh predicted the pinch off more accurately, it did not model the overall curvature well, the free surface had several bumps and did not appear smooth.

4.6 Finalized Algorithm

After gaining knowledge from the numerical studies in Sections 4.3, 4.4, and 4.5 a finalized algorithm has been reached to accurately predict the EWOD droplet cutting problem. Since it has been shown that a CLSVOF method including the effects of hysteresis is beneficial for the present study, the hysteresis deflection angle, Δ_{hys}, still has to be quantified. The idea is to obtain a hysteresis coefficient, K_{hys}, that results in an accurate prediction of the pinch-off time. For the present study, a hysteresis coefficient of K_{hys} = 0.008, yields the most accurate results. A hysteresis coefficient of K_{hys} = 0.008, results in an equivalent hysteresis deflection angle of Δ_{hys} = 6.99°. These finding are in contrast with [2] which found the optimal hysteresis coefficient to be K_{hys} = 0.09, and hysteresis deflection angle to be Δ_{hys} =6.4°. The reasoning behind different hysteresis coefficient comes from the diverse methods used to implement the hysteresis coefficient. Also equation (3.33) that is used to estimate the hysteresis coefficient is very sensitive to the input parameter, the hysteresis deflection angle, as showed in Figure 4.2.

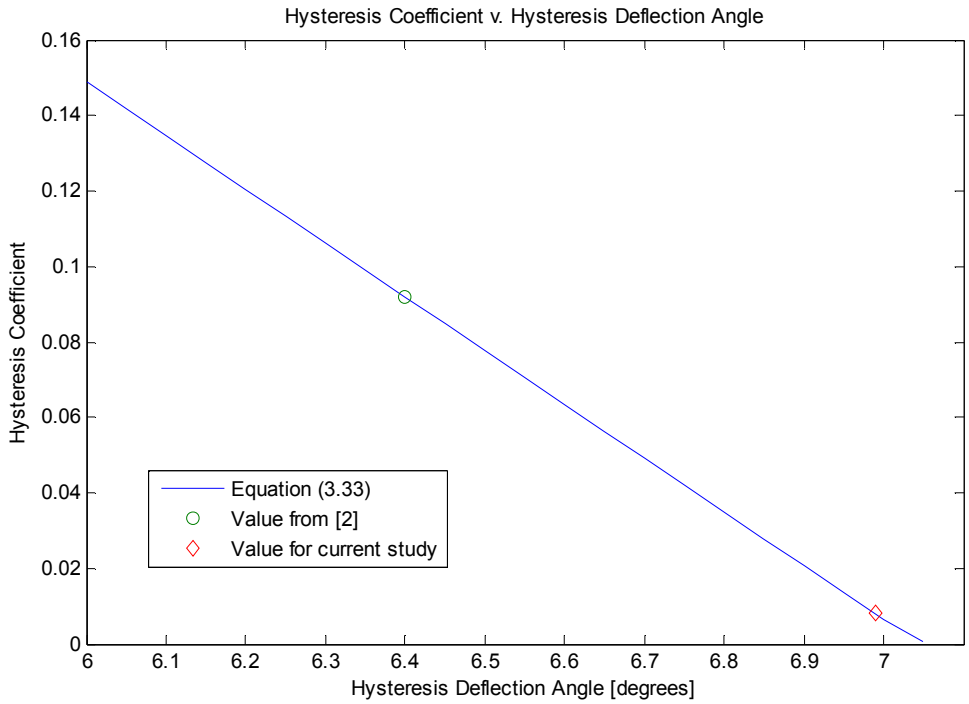

Figure 4.2. Hysteresis Coefficient versus Hysteresis Deflection Angle.

The pinch off time associated with using a value of K_{hys}=0.008 is 136.5 ms. Please note that the values from Table 4.2 were obtained using the above hysteresis coefficient.

The correct hysteresis coefficient has been obtained. The results for the EWOD droplet cutting problem are shown in Figure 4.5. The timing of the droplet motion is in agreement with the experimental data showed in Figure 4.6. When the droplet starts to spread the neck starts to develop, but it doesn't bulge as in the case where hysteresis is ignored, see Figure 4.4(a). As the droplet continues to spread the neck becomes very thin, as shown in Figure 4.5(e) and 4.6(b). The pressure difference caused by the voltage actuation keep the droplet spreading until the neck snaps. Once the neck snaps two separate droplets are formed with identical volume that rest on the two electrodes actuated by 25 V. As in Section 4.3, mass conservation was checked and 99.99% of the mass is preserved. This is an impressive improvement from the

mass conservation results mention in section 4.3. The mass of the fluid is preserved due to the addition of VOF free surface tracking in the CLSVOF method.

However the results obtained reveal that the overall shape and curvature of the free surface does not match exactly with the experimental results from [3]. In comparison of Figures 4.5 and 4.6, the present numerical model has a square type look to the droplets. Especially in comparison when the experiment is finish, as shown by comparison of Figure 4.5(f) and 4.6(c). Several attempts were made to remedy this problem numerically, but due to the assumptions made in Chapter 3 regarding the implementation of hysteresis, the current model is an approximation. The current numerical model accurately predicts the fluid displacement and correct pinch-off time, while completely conserving mass.

4.7 Parametric Study

4.7.1 Effect of Density

In this section, the effects of liquid density on the EWOD cutting problem are investigated. To see the sole effect of density in the results, all other parameters were kept constant as in Table 4.1. By inspection of Equation (3.31), it is expected that when the fluid density is decreased the rate of fluid acceleration should increase. Conversely if the fluid density is increased the rate of fluid acceleration should decrease. As mentioned in Chapter 3, Equation (3.31) is vital to accurately predicting the pinch-off time.

For the present study, four different values for liquid density have been simulated. The four values of liquid density used are 0.5, 0.75, 1.25, and 1.5 times the reference value of 996.93 kg/m^3 given in Table 4.1. In each of the four simulations, the pinch-off time, t^*, has been recorded. The results are shown in Table 4.3.

Table 4.3. Parametric study, effect of density.

ρ / ρ_{ref}	ρ [kg/m^3]	t^* [ms]
0.5	498.47	80.0
0.75	747.70	115.7
1.25	1246.16	156.7
1.5	1495.40	182.7

As shown the results are in agreement with the expected outcome, clearly as density increases the pinch off time decreases. Figures 4.7 and 4.8 are sample images from the simulations conducted in this section. Figure 4.7(b) shows the neck starting to thin while the droplet is being spread after only 51.4 ms, when ρ / ρ_{ref} = 0.5. In comparison, Figure 4.8(b) the neck starts to thin around 120.3 ms, when ρ / ρ_{ref} = 1.25. These results show the dramatic effect the density of the liquid has on the simulation of the EWOD droplet cutting problem.

4.7.2 Effect of Liquid Viscosity

The effects of varying liquid viscosities are investigated in this section. The key is to understand how viscosity affects fluid flow. The liquid viscosity and flow rate of fluid are related by the capillary number, which is given by [20]:

$$C_a = \frac{\mu U}{\sigma} \tag{4.1}$$

where U is the velocity scale. In theory an increase in the dynamic viscosity should relate to a decrease in the fluid flow rate, thus resulting in a larger pinch off time. As with Section 4.7.1 all other parameters are kept constant during the simulations. The dynamic viscosities are set to

0.5, 5, 10 and 15 times the reference viscosity in Table 4.1. The results from the simulations are reported in Table 4.4.

Table 4.4. Parametric study, effect of viscosity.

μ / μ_{ref}	μ [g/m*s]	t^* [ms]
0.5	0.45	104.0
5	4.45	410.8
10	8.90	681.2
15	13.35	873.6

The results are in accordance with the expected values. However the pinch-off time increases at a fast rate, greater than that expected. A parametric study on liquid viscosity in [16] on a different numerical problem found no significant variation in results when liquid viscosity was increased. From simulations ran in the present study, any dynamic viscosity greater than μ / μ_{ref} = 15, resulted in fluid not being able to cut into two separate droplets. The fluid would spread, but there was not a large enough pressure difference to overcome the viscous forces and cause the droplet to split. Even though viscosity didn't change, this is similar to a numerical study on modeling a EWDO device [21], where a minimum actuation voltage was needed to start the motion of the fluid. In that study the voltage was not large enough for the pressure difference to cause the droplet to move.

Figures 4.9 and 4.10 are sample images from the simulations conducted in this section. In Figure 4.9 the viscosity is μ / μ_{ref} = 0.5, a thin neck is starting to form around 70 ms, Figure 4.9(b), while after 120 ms, Figure 4.9(c), the fluid is at rest on top of each 25 V electrode. This is in contrast to Figure 4.10 where the viscosity is μ / μ_{ref} = 15. It takes nearly 600 ms for the

necking to occur, Figure 4.10(b), while the fluid does not rest in its final position until 1000 ms. This simulation is extremely slow, roughly 6 times slower than using the reference dynamic viscosity.

4.7.3 Effect of Surface Tension Coefficient

As mentioned in Chapter 2 surface tension is the driving force of the EWOD droplet motion and is one of the major factors affecting the pinch off time. To study the full effect surface tension has on the numerical model, various surface tension coefficients are used. They are 0.5, 1.5, 2, and 2.5 times the reference surface tension coefficient. As with Sections 4.7.1 and 4.7.2, the reference value is taken from Table 4.1. By analysis of Equation (3.26), the surface tension coefficient has a direct impact on the volume surface force. Due to the CSF model and the use of the volume surface force in computing fluid acceleration, it is expected that a larger surface tension coefficient should create a larger pressure difference, thus accelerating the motion of the fluid. Table 4.5 below lists the results from the simulations ran in this section.

Table 4.5. Parametric study, effect of surface tension coefficient.

σ / σ_{ref}	σ [J/m^2]	t^* [ms]
0.5	0.03600	231.4
1.5	0.10799	100.8
2.0	0.14398	81.9
2.5	0.17998	70.2

As expected from the knowledge in Chapter 3, the surface tension coefficient does have a direct and significant impact on the pinch off time. The increase in surface tension coefficient does in fact accelerate the motion of the fluid causing the pinch off to occur earlier in the simulation. A

timeline view of two of the simulations is shown in Figures 4.11 and 4.12. Figure 4.11 was run using σ / σ_{ref} = 0.5 and Figure 4.12 was run using σ / σ_{ref} = 2.5. Both figures differ in relationship to the initial spreading and necking of the droplet. By the time the droplet in Figure 4.11(a) starts to spread, the droplet in 4.12(b) is already starting to form a small neck. And thus this increase in the speed of the droplet motion results in differing pinch off and final resting times, as shown in comparison of Figure 4.11(c) and 4.12(c).

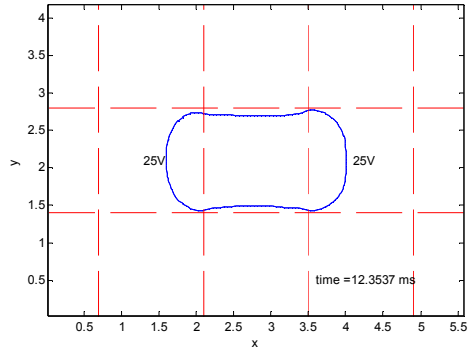

(a)

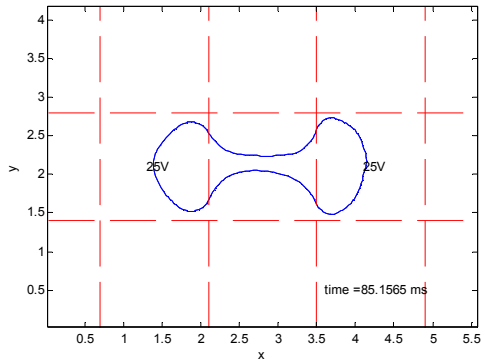

(b)

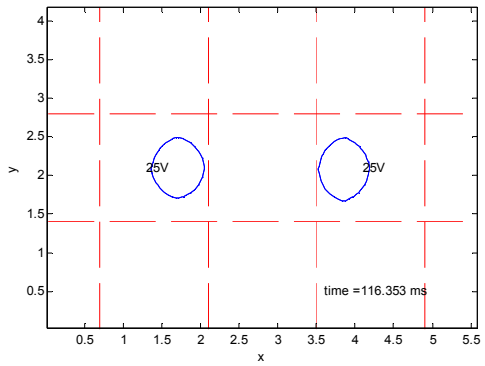

(c)

Figure 4.3. EWOD simulation, LS method. (a) 12.4 ms, (b) 65.2 ms, and (c) 116.4 ms.

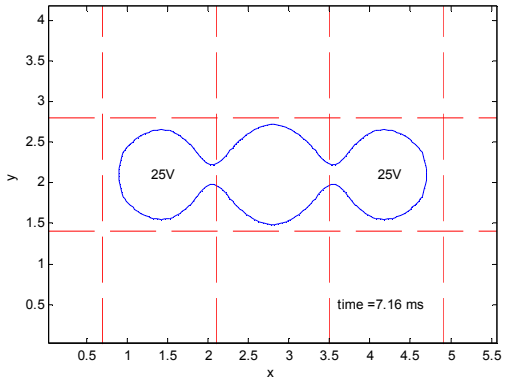

(a)

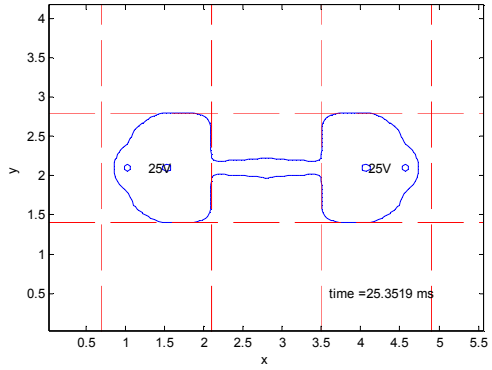

(b)

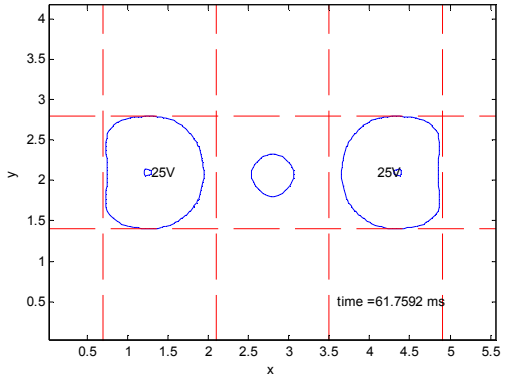

(c)

Figure 4.4. EWOD simulation, no hysteresis. (a) 7.2 ms, (b) 25.4 ms, and (c) 61.8 ms

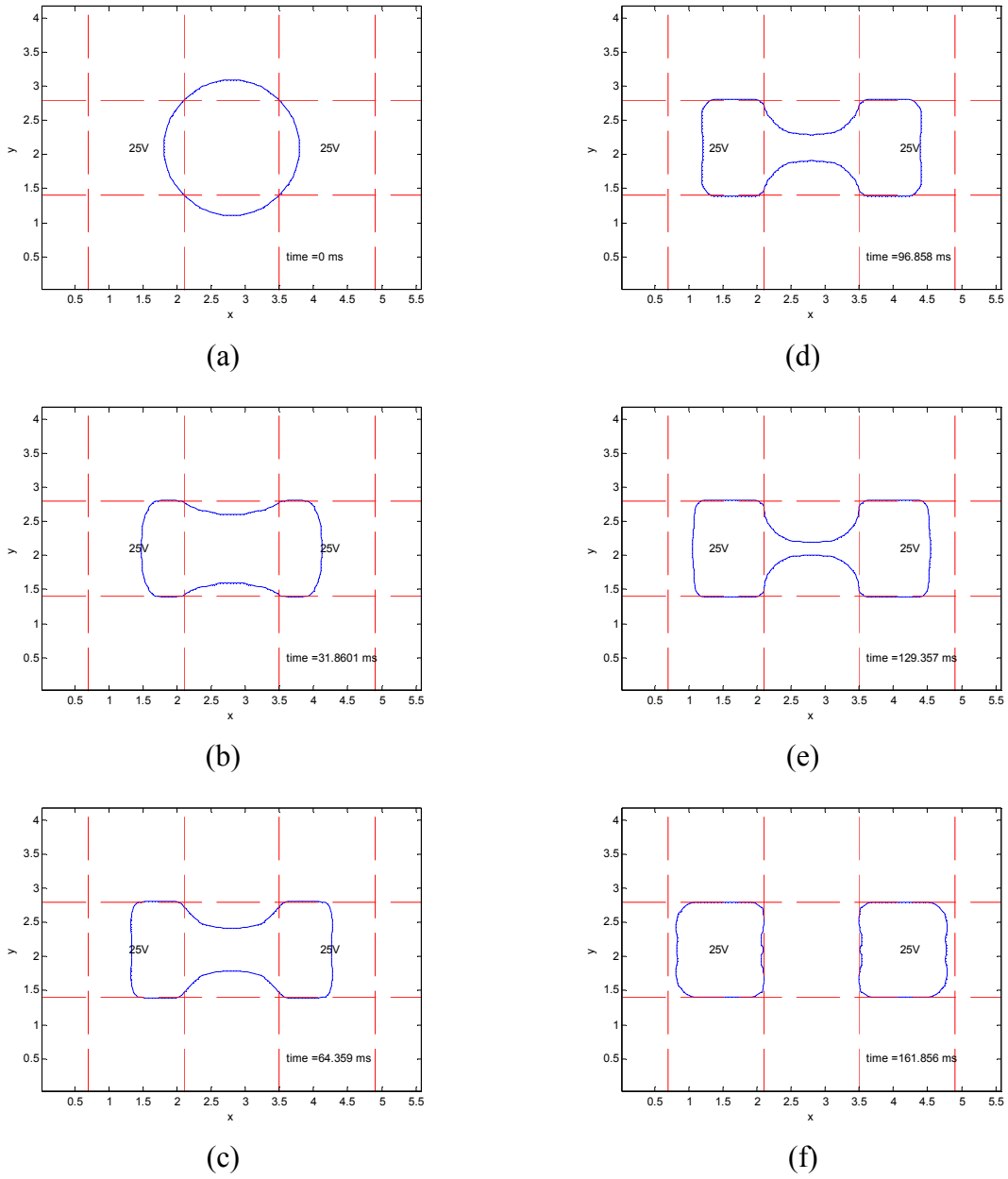

Figure 4.5. EWOD simulation, finalized algorithm. (a) 0 ms, (b) 31.6 ms, (c) 64.3 ms, (d) 96.6 ms, (e) 129.4 ms, and (f) 161.9 ms.

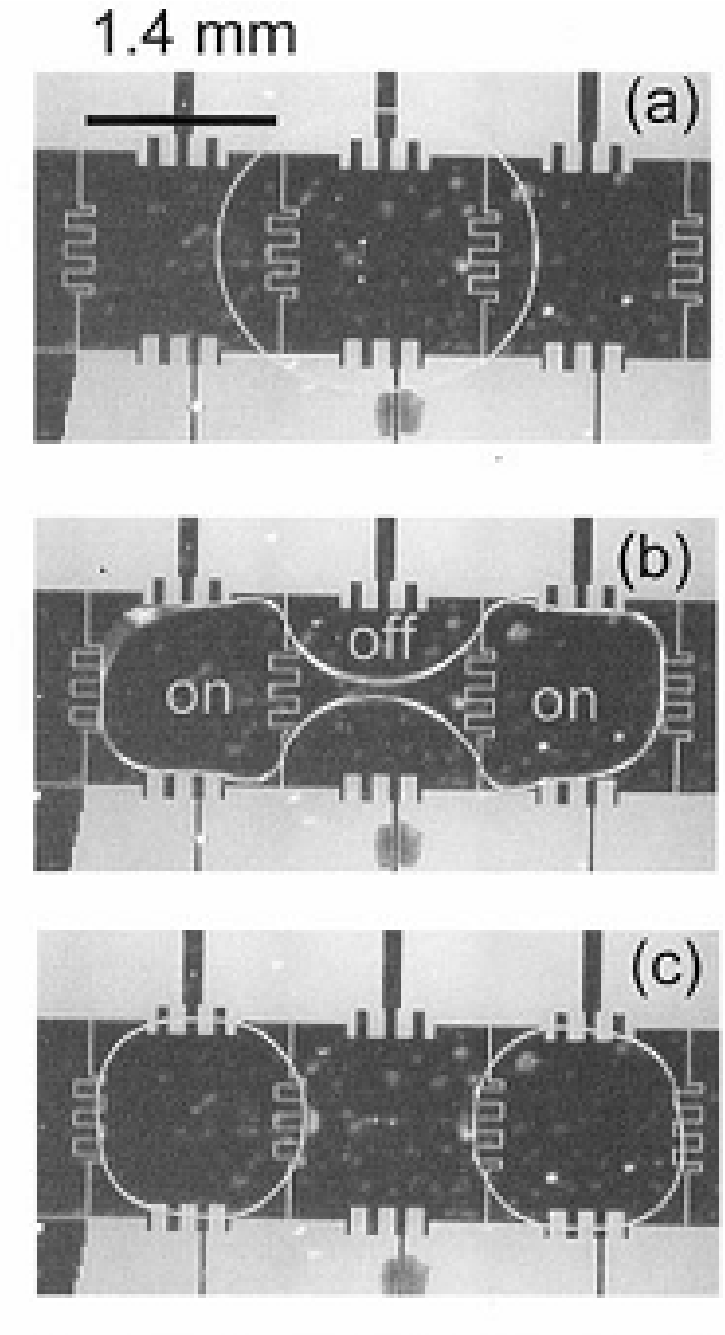

Figure 4.6. Experimental Results for EWOD Cutting Problem. (source: [3]). (a) 0 ms, (b) 133 ms, (c) 267 ms.

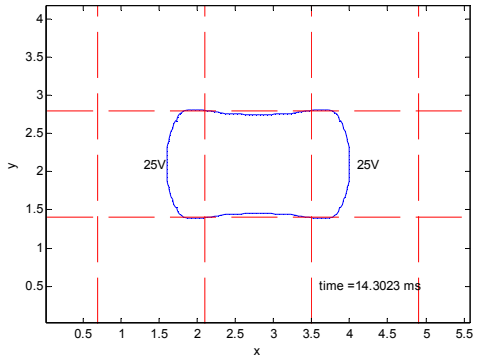

(a)

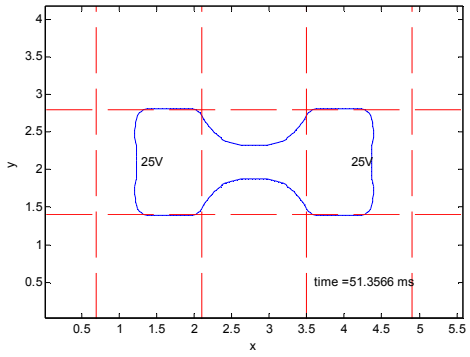

(b)

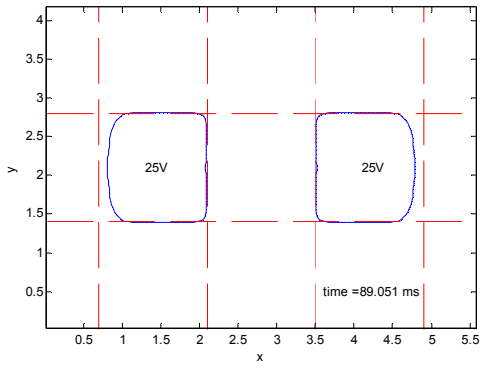

(c)

Figure 4.7. EWOD simulation, ρ / ρ_{ref} = 0.5. (a) 14.3 ms, (b) 51.4 ms, and (c) 89.1 ms.

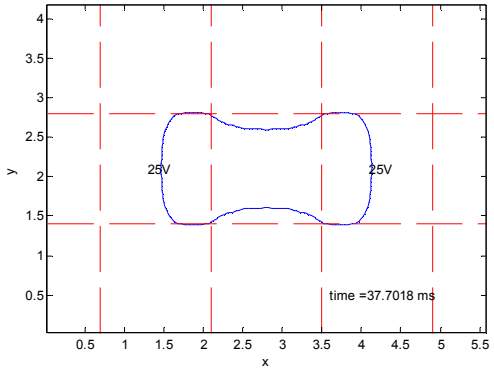

(a)

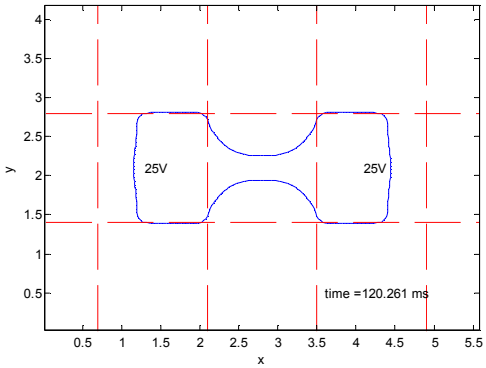

(b)

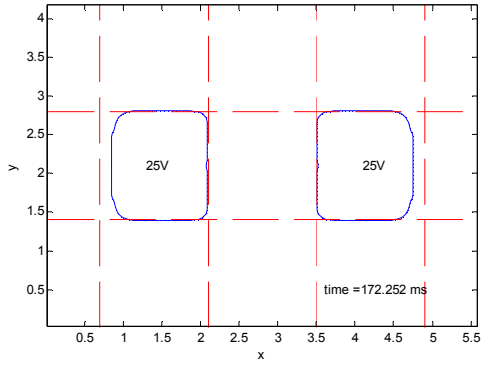

(c)

Figure 4.8. EWOD simulation, ρ / ρ_{ref} = 1.25. (a) 37.7 ms, (b) 120.3 ms, and (c) 172.3 ms.

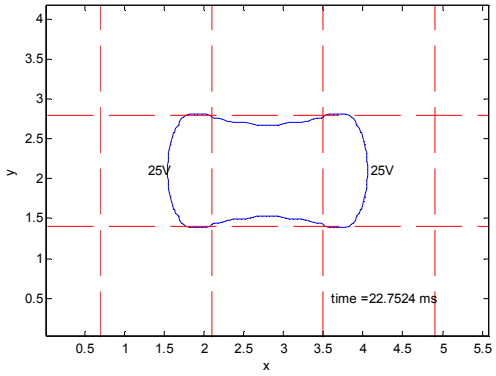

(a)

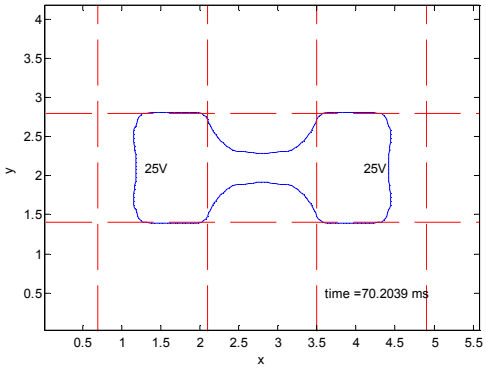

(b)

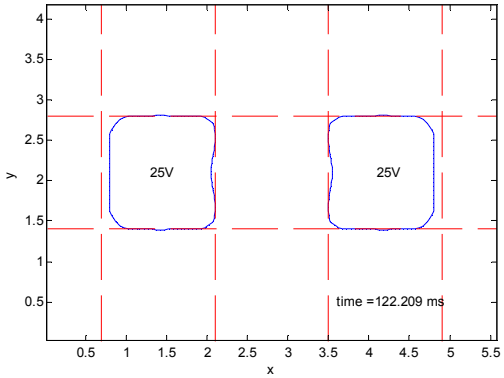

(c)

Figure 4.9. EWOD simulation, μ / μ_{ref} = 0.5. (a) 22.8 ms, (b) 70.2 ms, and (c) 122.2 ms.

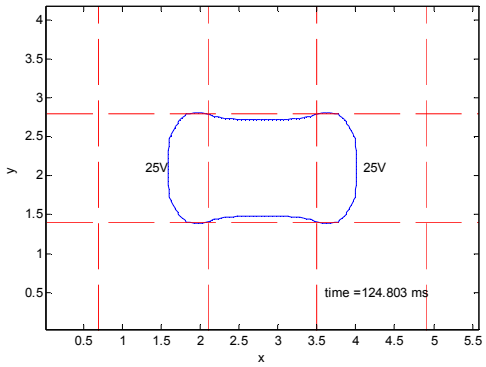

(a)

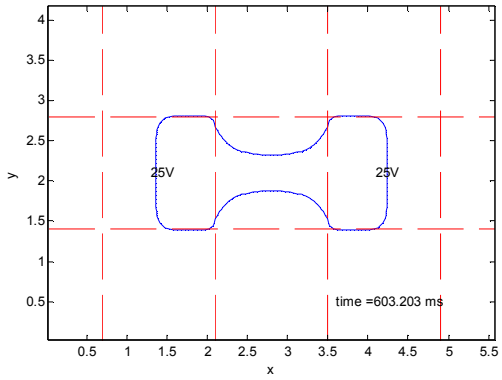

(b)

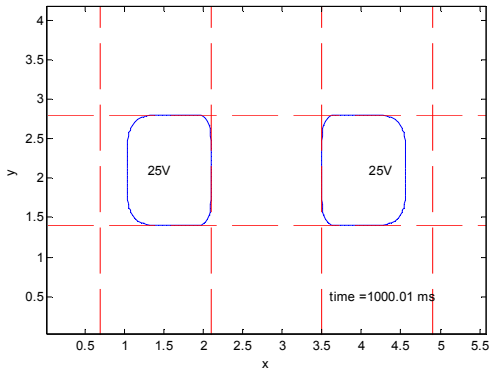

(c)

Figure 4.10. EWOD simulation, μ / μ_{ref} =15. (a) 124.8 ms, (b) 603.2 ms, and (c) 1000 ms.

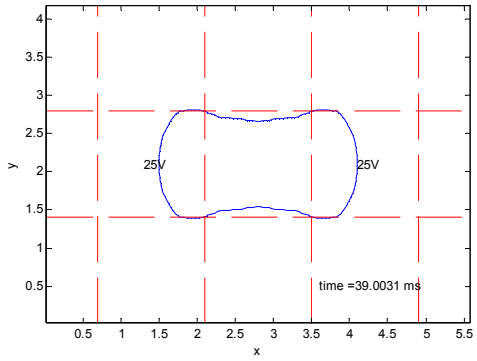

(a)

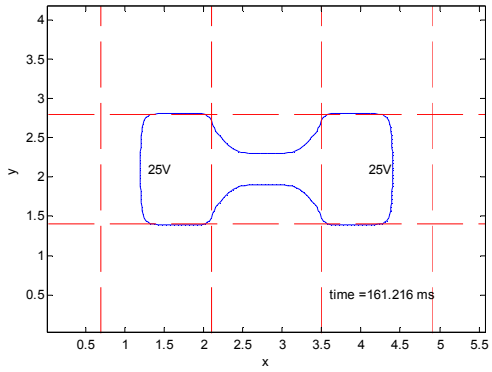

(b)

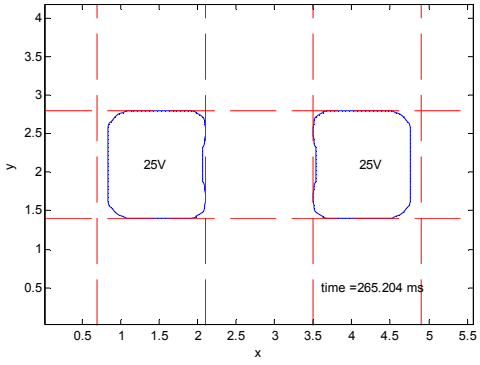

(c)

Figure 4.11. EWOD simulation σ / σ_{ref} = 0.5. (a) 39.0 ms, (b) 161.2 ms, and (c) 265.2 ms.

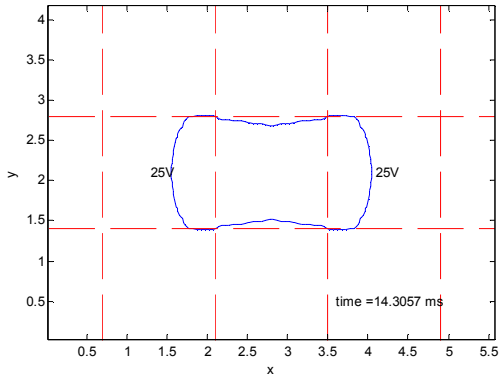

(a)

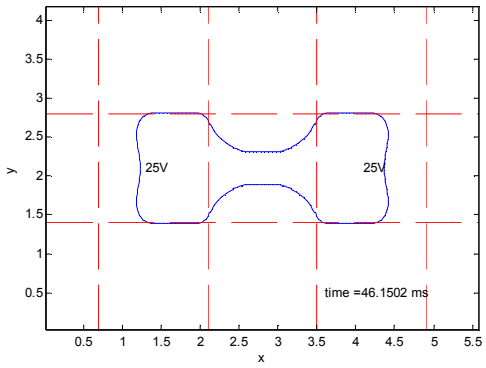

(b)

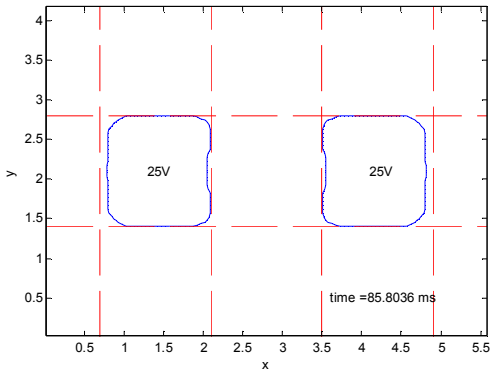

(c)

Figure 4.12. EWOD simulation σ / σ_{ref} = 2.5. (a) 14.3 ms, (b) 46.2 ms (b), and (c) 85.8 ms.

CHAPTER 5

CONCLUSIONS AND FUTURE WORK

The results obtained from the present numerical study of modeling a parallel plate EWOD device were presented. The CLSVOF method along with the CSF model has been applied for the current numerical simulations. Various numerical methods and techniques have been used to test the validity of the current model. The finalized algorithm does accurately predict the fluid displacement, pinch-off time, and final resting of the droplet of water within a EWOD device. The pinch-off time of 136.5 ms has an error of 5.8% compared with the experimental results in [3]. Based on the understanding of assumptions and approximations made in the current numerical model, 5.8% error is within an acceptable range.

A parametric study to test the influences of a variety of fluid properties, such as density, viscosity, and surface tension, was performed. The phenomenon observed was that the droplet accelerated and pinched off earlier when the density was decreased. The viscosity of fluid had a profound impact of the physics while it was observed that an increase in viscosity greatly decreased the rate of flow of the droplet. Also once the viscosity becomes much larger than 15 times the reference value, such as in oils, the viscous force becomes too large and the droplet cannot split. In contrast to viscosity, when the surface tension coefficient was increased, the rate of flow also increased resulting smaller pinch off times and the droplet resting in its final place sooner. By performing this parametric study using fluid properties, a greater understanding of the physics related to a EWOD device, and of the numerical model has been acquired.

The current research has the potential to be investigated further. Future study can be done in the area to find a method to solve for the fluid flow while keeping the curvature and shape of the droplet to match the experimental results. Also there is room for improvement for

modeling the effect of hysteresis, and possibly model the friction with the Teflon surface using a contact line pinning method similar to that used in [21]. The next step to the current computer code is to implement the program studying different EWOD problems. The current model has the potential to be used to solve a reservoir cutting problem, where smaller droplets are extracted from a larger reservoir droplet [3]. This problem requires timing based actuation, which is completely reasonable to be solved using the computer code in the present study.

APPENDIX A

CODE EXECUTION

The programming used in present study was written in FORTRAN for the UNIX environment. However two MatLab programs were written, *contactangle_curve.m* and *ewodhysteresis.m*. These MatLab programs were used compute the effects of contact angle saturation and hysteresis. Several numerical values were computed from these programs and then manually inserted into the FORTRAN program. In setting up a problem for computation, the user must supply an *input* file. This file contains the problem geometry, initial conditions, fluid properties, numerical parameters, and the free surface tracking scheme, either the LS or the CLSVOF. The information from the *input* file is fed to the compiled executable file, *ripple*. The main FORTRAN program groups the variables into format-free namelists. Modifications to original CLSVOF code were only made to two namelists, *srrfce.f* and *tenion.f*. The hysteresis coefficient was applied to the fluid acceleration in *srrfce.f,* and *tension.f* was modified to account for electrode location, fluid direction, and the effect of hysteresis in the CSF method. A sample *input* file and the details of the modifications are given in Appendix B.

The calculations are performed on the High Performance Computing (HPC) environment at The University of Texas at Arlington. The system consists of 840 processors with more than 90 Terabytes of aggregate storage. The computational nodes the HPC utilizes are Intel Core i7 processors. To run the program four files are required to be placed in a same directory: the *input* file, the *file_nam.dat* file which contains the number and names of output data, the *bjob* file which contains the load sharing facility (LSF) instructions, and the compiled executable, *ripple*. While program is running it periodically creates a data file. This data file has the form *ripp*.dat* or *ripp*.da*. All the relevant data specified is created at the time instant according to the frequency specified in the *input* file. The *file_nam.dat* file contains the number of files to be generated, and thus the total run time of the simulation. Each output data file contains the solutions in a specified format as follows:

1. The first and last real cells in the x- and y-direction
2. Location of the left side of each computational cell in the x-direction of the

lower side of each computational cell in the y-direction

3. Data : the velocity in the x-direction, the velocity in the y-direction, the volume fractions (VOF function value), the level set (LS) function value, the enthalpy, and the pressure.

A sample output data file is given in Appendix B.

In the present study, the post processing of the data obtained from the simulation was done in MatLab. A MatLab program has been created that loads the *ripp*.dat* and *ripp*.da* files. This program is also what is used to create various plots and graphs of the numerical simulations.

APPENDIX B

SAMPLE INPUT AND OUTPUT

B.1. Sample INPUT

A sample *input* file is shown below

```
EWOD device test by kevin tully
 $numparam
   alpha=1.0,
   conserve=.false.,
   autot=1.,
   delt=0.25e-2,
   dtmax=0.25e-1,
   twfin=1000.0,
   con=0.3,
   fcvlim=0.5,
   idiv=1,
   dmpdt=3000000.0,
   prtdt=1000000.0,
   pltdt=6.5e-1,
   sym=.true.,
   kt=3,
   kb=1,
   kl=3,
   kr=3,
 $end
 $fldparam
   gy=0.0,
   icyl=0,
   isurf10=1,
   psat = 0.0,
   xnu=8.927407e-4,
   rhof=0.99693,
   sigma=0.07199,
 $end
 $mesh
   nkx=1,
   xl=0.0,5.6,
   xc=2.8,
   nxl=56,
   nxr=56,
   dxmn=0.05,
   nky=1,
   yl=0.0,2.1,
   yc=1.05
   nyl=21,
   nyr=21,
   dymn=0.05,
 $end
 $obstcl
   nobs=0,
 $end
 $freesurf
   nfrsrf=2,iequib=0,
```

```
  fc1(1)=-1.0, ifh(1)=1,
  fa1(2)=-5.6, fa2(2)=1.0,
  fb1(2)=0.0, fb2(2)=1.0, fc1(2)=6.86, ifh(2)=0,
$end
$graphics
  plots=.true., dump=.false.,
  iout = 0, 1, 0, 0, 0, 0, 0, 0, 0, 0, 0, 0, 0,
        0, 0, 0, 0, 0, 0, 0, 0, 0, 0, 0, 0, 0,
        0, 0, 0, 0, 0, 0, 0, 1, 0, 0, 0, 0, 1,
  iysymplt=0,
$end
$heateq
  heat= .false.,
  ischeme=3,
$end
$coupled
  lsvof=.true.,
  ls=.false.,
$end
```

B.2 Sample OUTPUT

The data files contains the solutions of the governing equations are named according to the *file_nam.dat* file. A sample output file and its explanations are given below.

```
0.00000E+000  <----- time

2, 112                    <----- 1st real cell, last real cell in x-direction

2,42                      <----- 1st real cell, last real cell in y-direction

0.00000E+000  <----- location of the left side of each computational

1.00000E-001          cell in the x-direction

2.00000E-001

3.00000E-001

4.00000E-001

5.00000E-001

6.00000E-001

.

.
```

.

0.00000E+000 <----- location of the left side of each computational

1.00000E-001 cell in the y-direction

2.00000E-001

3.00000E-001

4.00000E-001

5.00000E-001

6.00000E-001

7.00000E-001

8.00000E-001

9.00000E-001

1.00000E+000

.

.

.

0.00000E+0,-4.50000E-1, 0.00000E+0, 1.00000E+6, 0.00000E+0, 0.00000E+0

0.00000E+0,-4.50000E-1, 0.00000E+0, 1.00000E+6, 0.00000E+0, 0.00000E+0

0.00000E+0,-4.50000E-1, 0.00000E+0, 1.00000E+6, 0.00000E+0, 0.00000E+0

0.00000E+0,-4.50000E-1, 0.00000E+0, 1.00000E+6, 0.00000E+0, 0.00000E+0

0.00000E+0,-4.50000E-1, 0.00000E+0, 1.00000E+6, 0.00000E+0, 0.00000E+0

. (comp. 1), (comp.2), (comp. 3), (comp. 4), (comp.5), (comp.6)

.

In the above six-column matrix, components from comp.1 to comp.6 show the following solutions:

comp.1: velocity component in x-direction

comp.2: velocity component in y-direction

comp.3: VOF function value

comp.4: LS function value

comp.5: enthalpy

comp.6: pressure.

REFERENCES

[1] Wang, Z., 2006, "Numerical Study on the Capillarity-Dominant Free Surface and Interfacial Flows,". Ph.D. dissertation, The University of Texas at Arlington.

[2] Walker, S. W., and Shapiro, B., 2006, "Modeling the Fluid Dynamics of Electrowetting on Dielectric (EWOD)," Microelectromechanical Systems, Journal of, **15**(4) pp. 986-1000.

[3] Sung Kwon Cho, Hyejin Moon, and Chang-Jin Kim, 2003, "Creating, Transporting, Cutting, and Merging Liquid Droplets by Electrowetting-Based Actuation for Digital Microfluidic Circuits," Microelectromechanical Systems, Journal of, **12**(1) pp. 70-80.

[4] Shapiro, B., Moon, H., Garrell, R. L., 2003, “Equilibrium behavior of sessile drops under surface tension, applied external fields, and material variations,” Journal of Applied Physics, **93**(9) pp. 5794-5811.

[5] Lin, J., Lee, G., Chang, Y., 2006, “Model Description of Contact Angles in Electrowetting on Dielectric Layers,” Langmuir, **22**(1) pp. 484-489.

[6] Lippmann, G., 1875, Ann. Chim. Phys., **5**pp. 494.

[7] Quinn, A., Sedev, R., and Ralston, J., 2005, “Contact Angle Saturation in Electrowetting,”. J. Phys. Chem. **109**(13) pp. 6268-6275.

[8] Johnson, R.W., 1998, "The Handbook of Fluid Dynamics," CRC Press LLC, Boca Raton, FL, U.S.A.

[9] Burdon, R.S., 1949, "Surface Tension and the Spreading of Liquids," Cambridge University Press, Cambridge, U.K., .

[10] Adam, N.K., 1944, "The Physics and Chemistry of Surfaces," Oxford University Press, Oxford, U.K., .

[11] Kothe, D., B., Mjolsness, R.C., and Torrey, M.D., 1994, "RIPPLE: A Computer Program for Incompressible Flows with Free Surfaces," LA-12007-MS.

[12] Hirt, C. W., and Nichols, B. D., 1981, "Volume of Fluid (VOF) Method for the Dynamics of Free Boundaries," Journal of Computational Physics, **39**pp. 201.

[13] Lu, M., 2000, "Numerical Modeling of Multi-Phase Surface Flow,". Ph.D. dissertation, The University of Texas at Arlington.

[14] Sussman, M., Smereka, P., and Osher, S., 1994, "A Level Set Approach for Computing Solutions to Incompressible Two-Phase Flow," Journal of Computational Physics, **114**(1) pp. 146-159.

[15] Sussman, M., and Fatemi, E., 1999, “Efficient, interface-preserving level set redistancing algorithm and its application to interfacial incompressible fluid flow”, Computers & Fluids, **20**(4) pp. 1165-1191.

[16] Takkallapally, S. K., 2009, "A Numerical Study on the Dynamics of Bubble Growth and Detachment from an Orifice,". Masters thesis, The University of Texas at Arlington.

[17] Kamiya, R., 2005, "A Numerical Study of Pendant Droplet Formation from a Capillary Tube,". Masters thesis, The University of Texas at Arlington.

[18] Brackbill, J. U., Kothe, D. B., and Zemach, C., 1992, "A Continuum Method for Modeling Surface Tension," Journal of Computational Physics, **100**(2) pp. 335-354.

[19] Torrey, M.D., Cloutman, L.D., Mjolsness, R.C., 1985, "NASA-VOF2D: A Computer Program for Incompressible Flows with Free Surfaces," LA-10612-MS.

[20] Hirasaki, G. J., and Yang, S. Y., 2002, “Dynamic contact line with disjoining pressure, large capillary numbers, large angles and pre-wetted, precursor, or entrained films,” Contact Angle, Wettability and Adhesion, **2**pp. 1.

[21] Walker, S. W., 2007, "Modeling, Simulating, and Controlling the Fluid Dynamics of Electro-Wetting on Dielectric,". Ph.D. dissertation, University of Maryland, College Park.

BIOGRAPHICAL INFORMATION

Kevin Tully received his Bachelor's degree in Mechanical Engineering from Texas Christian University, Fort Worth, Texas, in May 2009. He received his Master's degree in Mechanical Engineering from The University of Texas at Arlington in May 2011. His areas of interests include computational methods, fluid dynamics and heat transfer.